Bull. Chem. Soc. Ethiop. **2025**, 39(1), 153-164. ISSN 1011-3924
© 2025 Chemical Society of Ethiopia and The Authors Printed in Ethiopia
DOI: https://dx.doi.org/10.4314/bcse.v39i1.13 Online ISSN 1726-801X

EFFECT OF (Zr, Ta) DOPING ON ELECTRONIC AND MAGNETIC PROPERTIES OF ZINC-BLENDE MGTE DMS COMPOUND: AB-INITIO APPROACH

M. Laghrissi[1,2*], M. Drissi El Bouzaidi[1,2,3], F. Goumrhar[1,2,4], L. Essebbahi[1,2] and R. Ahl Laamara[1,2]

[1]LPHE, Modeling & Simulations, Faculty of Science, Mohammed V University, Rabat, Morocco
[2]CPM, Centre of Physics and Mathematics, Faculty of Science, Mohammed V University, Rabat, Morocco
[3]National School of Architecture of Tétouan (ENA), Tétouan, Morocco
[4]Higher School of Education and Training of El Jadida (ESEF), Chouaib Doukkali University, El Jadida, Morocco

(Received July 23, 2024; Revised September 7, 2024; Accepted September 9, 2024)

ABSTRACT. This study utilizes density functional theory (DFT) and the Korringa-Kohn-Rostoker coherent potential approximation (KKR-CPA) to explore the effects of zirconium (Zr) and tantalum (Ta) doping on the electronic and magnetic properties of zinc-blende MgTe. The electronic configurations of $Mg_{1-x}(TM)_xTe$ (TM = Zr, Ta) were analyzed, revealing that Zr induces magnetic behavior with near-total spin polarization, while Ta doping leads to metallic behavior with partial polarization. The variations in magnetic moments are largely determined by impurity concentrations, with ferromagnetic stability in both systems driven by a double exchange interaction mechanism. Additionally, Curie temperatures exceeding room temperature were observed for specific doping concentrations. These results suggest significant potential for MgTe-based materials in spintronic applications. The findings further illustrate that Zr-doped alloys display half-metallicity, making them especially promising for future spintronics device development.

KEY WORDS: DMS, KKR-CPA, Polarization, Metallic behavior, Curie temperature, Double exchange, Spintronic

INTRODUCTION

Diluted magnetic semiconductors (DMS) doped with transition metals (TM) or elements of phantom d^0 or rare earth have emerged as intriguing materials, displaying novel phenomena driven by these elemental substitutions. The incorporation of such elements results in profound changes to the mechanical, thermal, optical, electronic, and magnetic properties of the systems under consideration [1, 2]. Consequently, DMS has gained significant attention and appreciation in the electronics industry, where they have been seamlessly integrated into numerous spintronic devices.

One of the most remarkable features of DMS is their distinct property of half-metallicity [3, 4], wherein they exhibit 100% spin polarization at the Fermi level for one spin direction. In addition, DMS demonstrate high Curie temperatures (T_c) exceeding room temperature [5, 6]. The simultaneous presence of half-metallicity and high Curie temperatures unlocks a myriad of possibilities, allowing the creation of devices capable of simultaneously storing and propagating information, thereby eliminating the need for separate devices.

DMS can be broadly categorized into four types: III-V, II-VI, II-IV, and IV-VI [7]. Notably, the Type II-VI DMS has found widespread applications in various fields, such as

*Corresponding authors. E-mail: mouloud_laghrissi@um5.ac.ma

optoelectronics [8], piezoelectronics, heterojunctions [9], thermoelectrics [9, 10], and solar cells [10], making it a versatile and promising material for future technological advancements.

Recently, the field of spintronics [10, 11] has played a pivotal role in driving the development of new materials that enable the inseparable manipulation of both electron spin and electrical charge [12, 13]. This interdisciplinary field has demonstrated practical applications in diverse areas, exemplified by the use of spin field-effect transistors (Spin-FETs) [14, 15], spin-based quantum computing [16], spin-orbit torque (SOT) devices [17], spin photodetectors [20], spin-based neuromorphic computing [18], and spin caloritronics [19]. Additionally, diluted magnetic semiconductors (DMS) such as GaN, SiC, and GeC [20], as well as diluted magnetic oxides like TiO_2, ZnO, and CeO_2 [21, 24], have emerged as promising candidates in the pursuit of spintronics-based technologies.

Considering the promising properties and applications of DMS, this paper aims to delve deeper into the unique characteristics of Type II-VI DMS and explore their potential for further advancements in spintronics and related fields. By investigating the mechanical, thermal, optical, electronic, and magnetic properties of Type II-VI DMS, we seek to contribute to the growing body of knowledge in this exciting area of research and foster innovations in the electronics industry. The findings presented here may pave the way for the development of cutting-edge spintronic devices with enhanced performance and efficiency, thereby driving the next generation of transformative technologies.

The MgTe material is a II-VI type from the family of DMS that plays an important role in various fields of physics. It also has a direct energy gap; this bandgap is relatively large compared with that of group IIB elements. Experimentally, it reached 3.49 eV, which is a greater value than that of CdTe 1.59 eV [25]. This can be explained by the absence of d-states in IIA compounds, which translates into a reduction of the state located at the valence band edge and a broadening of the band gap. This mechanism makes MgTe an easy element to dope for both n- and p-types [26]. This compound can crystallize in four crystalline phases, including zinc-blende (ZB), rock-salt (RS), wurt-zite (WZ) and nickel arsenide (NiAs) [27]. All these characteristics make MgTe a promising element, which is showing its potential in the production of optoelectronic devices [28]. It is also used for high-speed fiber optic communication networks [29], photovoltaic cells and photodetectors [30]. The high hygroscopicity of MgTe did not prevent Boulanger and his colleagues from synthesizing these compounds and injecting them with Cr for the electron paramagnetic resonance (EPR) studies [31]. On the other hand, Kuhn's team [32] affirmed in an extensive study that when using ultraviolet excitation at room temperature, MgTe:Mn did not show any photoluminescence and that this compound exhibits a high refractive index. Moreover, in a theoretical study using the generalized gradient approximation (GGA), Behbahani and co-workers reported that Ti-doped samples became more efficient in optoelectronic devices, as well as that the presence of distinctive half-metallic properties and a high Curie temperature make these materials good candidates for spintronics applications [33].

Given these promising properties, numerical simulations play a crucial role in further advancing our understanding of MgTe and similar materials. Numerical simulation allows better consideration of needs and constraints as well as rapid modification of parameters at lower cost. The use of DFT, DFT+U, or DFPT has become a major asset in the field of materials science to predict the different properties of various compounds before moving on to experimental work, especially for those with specific characteristics. In some cases, it is necessary to combine both theory and experiment to better understand certain phenomena, thereby enhancing the development of materials with tailored properties for advanced technological applications [34-39].

In the present work, we have focused on studying the electronic, magnetic, and half-metallic properties of MgTe doped at specific concentrations (x = 0.04, 0.08, 0.12, and 0.20) by two transition metals (TM), zirconium (Zr) and tantalum (Ta), which have different electron

numbers and behave differently in the host semiconductor. In order to investigate the appearance of half-metallic character, Curie temperature variations, and the effect of different impurity concentrations in $Mg_{1-x}(TM)_xTe$, a detailed study has been carried out using the general gradient approximation (PBE-GGA) to obtain theoretical data that can be compared with future experiments in the field of spin-electron devices. Our paper is partitioned as indicated: the second section is dedicated to a thorough study of the calculation procedure and the structural properties. The third section presents a general analysis of the electronic, magnetic and half-metallic properties of the $Mg_{1-x}Zr_xTe$ and $Mg_{1-x}Ta_xTe$ compounds. Finally, the last section summarizes the results of this work and draws conclusions.

CALCULATION METHOD AND STRUCTURAL PROPERTIES

In our investigation of the electronic and magnetic properties of MgTe doped with zirconium (Zr) and tantalum (Ta), we conducted ab-initio calculations based on density functional theory (DFT). The computational framework relied on the Korringa-Kohn-Rostoker (KKR) method combined with the coherent potential approximation (CPA) [40] to accurately model the disordered alloys. In the KKR-CPA method, impurity concentrations can be calculated within the same computational framework by averaging the electronic properties. This approach eliminates the need to use a supercell model to simulate disorder in the system. The generalized gradient approximation (GGA) was employed, utilizing the Perdew, Burke, and Ernzerhof (PBE) parameterization [41] to account for exchange-correlation effects. All calculations were performed using the MACHIKANEYAMA2002V10 package, a specialized computational tool developed by Akai at Osaka University, Japan [42], which integrates these methods and approximations seamlessly.

To incorporate relativistic effects, we used the scalar relativistic approximation (SRA), which considers relativistic corrections to electron dynamics without full relativistic complexity, ensuring both accuracy and computational efficiency. For convergence, we used a dense k-point mesh, with up to 500 k-points in the irreducible part of the first Brillouin zone, ensuring a precise description of the ground state properties.

The MgTe compound, crystallizing in the Zinc-Blende (ZB) structure with the space group $F\bar{4}3m$ (216), serves as the host material in our study. The lattice parameter was fixed at 6.19 Å, a value derived from both theoretical and experimental studies by Noor *et al.* [43], and corresponds to the minimum total energy configuration, as reported in ref. [44]. The unit cell of MgTe comprises two atoms per cell: magnesium (Mg, Z = 12) at the (0, 0, 0) position and tellurium (Te, Z = 52) at the (1/4, 1/4, 1/4) position. To enhance the accuracy of our electronic structure calculations, empty spheres (ES) with an atomic number of zero were introduced at interstitial sites, as shown in Figure 1, to improve the potential representation within the crystal.

Regarding the dopants, zirconium (Zr) with an electronic configuration of $[Kr]5s^24d^2$, and tantalum (Ta) with an electronic configuration of $[Xe]6s^25d^34f^{14}$, were selected to investigate their influence on the electronic and magnetic properties of MgTe. These dopants were incorporated into the MgTe matrix, and their impact on the system's electronic structure and magnetic behavior was meticulously analyzed through the computational methods described above.

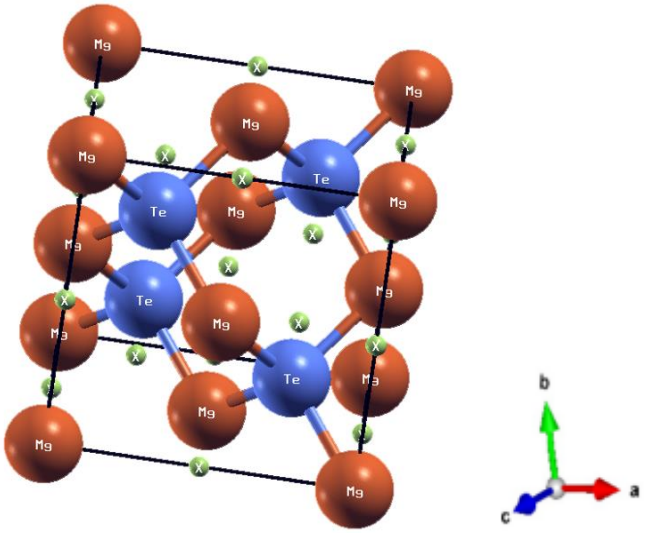

Figure 1. The MgTe unit cell is composed of brown-colored Mg atoms, blue-colored Te atoms and green-colored empty spheres [39].

RESULTS AND DISCUSSION

Firstly, recall that the electronic structure of pure compound MgTe's, as stated in the references [44, 45], reveals a semiconductor with a direct bandgap theoretically estimated at 1.75 eV [44]. Furthermore, this material exhibits an intrinsic non-magnetic nature.

In the remainder of this section, by using ab-initio calculations, we have studied the effect of doping the MgTe compound with transition metals (TM) such as zirconium (Zr) and tantalum (Ta) to improve its electronic and magnetic properties. The optimized lattice constants after doping are listed in Table 1, which was used to calculate all the data in this work. The total and partial DOS of doped $Mg_{1-x}(TM)_xTe$ where (x = 0.04, 0.08, 0.12 and 0.20) are plotted in Figure 2.

The results show that for all the doping concentrations, both compounds exhibit nonzero magnetic moments. Figure 2 shows that there is a break at the DOS symmetry while a spin polarization is found at E_F. This asymmetry is due to the ferromagnetic behavior of the alloys. At Fermi level $E_{F,}$ we see clearly that new apexes corresponding to Zr (4d) appear in the majority spin states, but they disappear in the minority spin states. In this regard, one sees that our compound is a half-metal. This behavior is created by the p – d hybridization between localized states around the Fermi level d-TM and p-Te. From the Figure 2, we note that the studied alloys $Mg_{1-x}Ta_xTe$ is metallic with magnetic behavior, which can be explained by the appearance of peaks located in the middle of the E_F in the minority and majority spin states without any band gap. The difference in the density of states curves at E_F of the two alloys is justified by the fact that Ta has one more valence electron in the d-layer. These d-states play a crucial role in determining the nature of conductivity and the characteristics of a DMS. When a transition metal atom is substituted at the cation site Mg, the d states of transition metal are tetrahedrally surrounded by four Te atoms; these states split into three degenerate states ($\boldsymbol{t_2}$) and two degenerate states (**e**) due to crystal field splitting. From Figure 2 (a and b), it's clear that the **e** states are less energetic than the $\boldsymbol{t_2}$ states, which confirms the tetrahedral environment of the alloys.

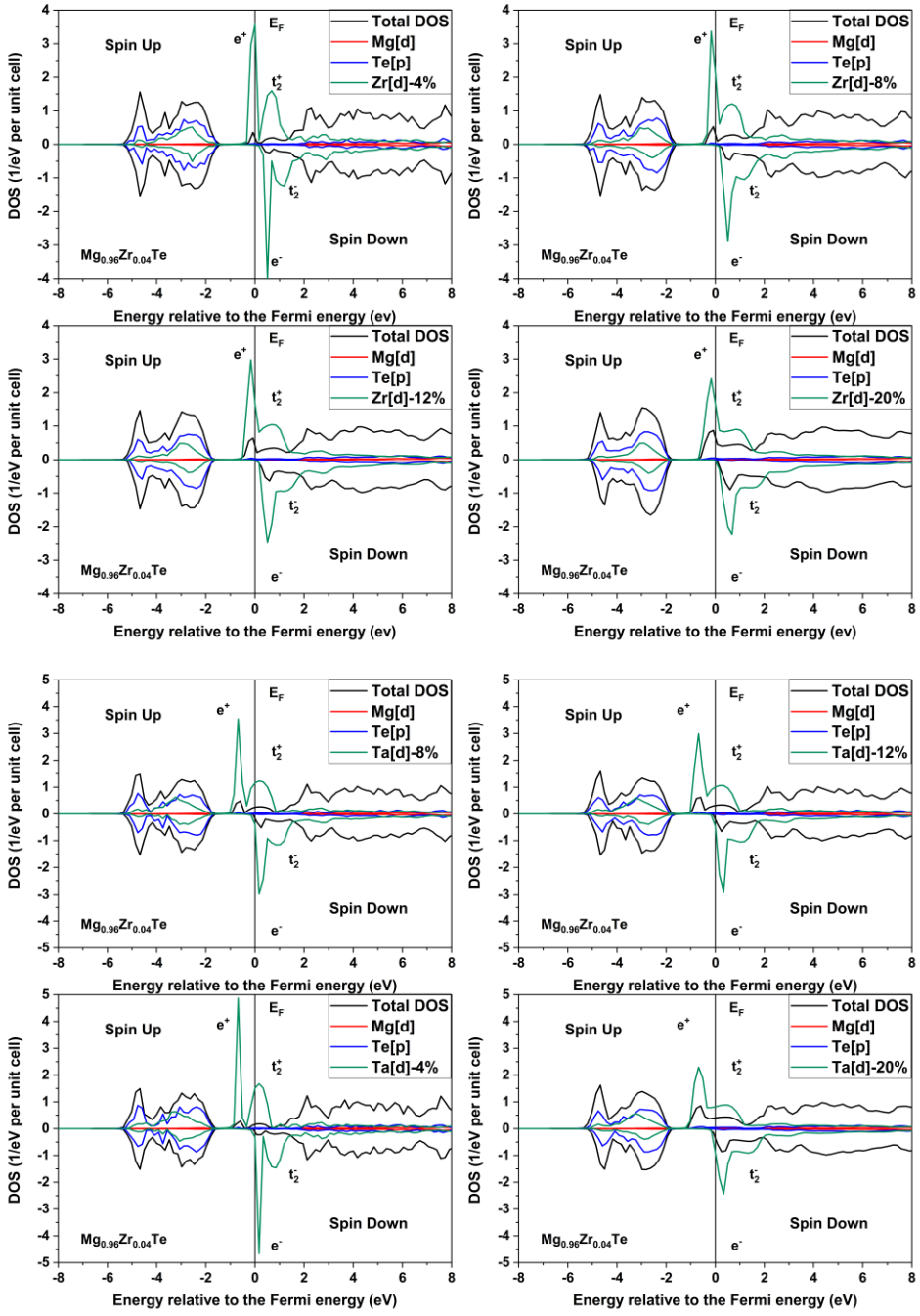

Figure 2. Total and partials DOSs of $Mg_{1-x}Ta_xTe$ and $Mg_{1-x}Zr_xTe$ compound (x = 0.04, 0. 08, 0.12 and 0.20).

It can also be noted that the occupancy of these e and t_2 bands is related to the number of electrons available in the d states. In the case of $Mg_{1-x}Zr_xTe$, the e^+ states are completely filled, while all other states are unoccupied. By increasing the number of electrons in d-Ta, the partially occupied states ⟦t_2⟧^+ and e^- cross the fermi level, giving rise to metallic behavior. By increasing the concentration, we notice a broadening and amplitude reduction of the d-TM peaks (Figure 3); this process contributes to gradually increasing the stability of the ferromagnetic states and is called the double exchange mechanism. This mechanism is caused by the strong hybridization that occurs between the d-states of the two transition metals and the p-states of Te [46].

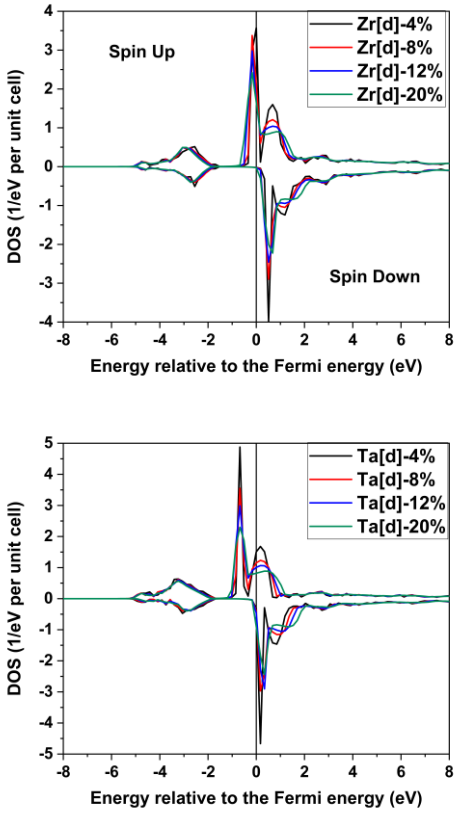

Figure 3. A concentration-based Partial DOS comparison of d-orbitals of Zr and Ta.

In order to examine the magnetic stability of these alloys, we compare between the energies of the ferromagnetic state E_{Ferro} identified by the same direction for all spins as noted $Mg_{1-x}(TM)_x^{\uparrow}Te$, while the state of disordered local moment (DLM) E_{DLM} identified as $Mg_{1-x}(TM)_{x/2}^{\uparrow}(TM)_{x/2}^{\downarrow}Te$ which is simulated by half of the impurity ion spinning upward and the remaining points spinning downward to make the total moment disappear. The energy difference is expressed as:

$$\Delta E = E_{DLM} - E_{Ferro} \quad (1)$$

Thus, data in Table 1 shows that for the two $Mg_{1-x}Zr_xTe$ and $Mg_{1-x}Ta_xTe$ components, the ferromagnetic phase is the most stable for all concentrations. However, starting from a 13% concentration of Zr, the antiferromagnetic phase becomes energetically more favorable, as observed in Table 1 where the ΔE for 20% Zr is a negative value. This method is the most used for theoretical study for different materials CdS [10, 17, 23, 25]. Table 1 also reveals that the variation of total and partial magnetic moments of the two alloys $Mg_{1-x}(TM)_xTe$ (TM= Zr or Ta) is close to each other. The p-d hybridization between the localized d-TM and p-Te states leads to the occurrence of magnetism in the Te and Mg sites. The dominant contributors to the total magnetic moment are the atoms of the TM, with a negligible effect of Mg and Te. The negative magnetic moment that appears in Te indicates that the MTe aligns in an antiparallel way with the MZr. However, it can be seen that increasing the TM concentrations significantly affects the total magnetic moments of the alloys.

Table 1. Variation of lattice constants, total and partial magnetic moments, ferro and DLM energies, the total energy difference, and stability phase of $Mg_{1-x}Ta_xTe$ and $Mg_{1-x}Zr_xTe$ compound (x = 0.04, 0. 08, 0.12 and 0.20).

TM	x %	a_0(Å)	Mtotal (μB)	M_{TM} (μB)	M_{Mg}(μB)	M_{Te} (μB)	ΔE	Stability phases
Zr	4	6,2707	-0.0691	1.1668	0.0031	-0.00001	0,0029	Ferro
Zr	8	6,2919	0.1467	1.2202	0.0063	-0.0002	0,0031	Ferro
Zr	12	6,3131	0.2246	1.2363	0.0090	-0.0011	0,0009	Ferro
Zr	20	6,3554	0.3811	1.2487	0.0136	-0.0057	-0,0062	DLM
Ta	4	6,2972	0.1041	1.6244	0.0040	0.0002	0.0034	Ferro
Ta	8	6,2866	0.2191	1.6826	0.0082	0.0007	0.0063	Ferro
Ta	12	6,3131	0.3342	1.7218	0.0119	0.0014	0.0131	Ferro
Ta	20	6,3343	0.5322	1.6588	0.0170	0.0077	0.0032	Ferro

As indicated in Table 2, we have calculated the spin polarization at the E_F by using the following equation (2) [47]:

$$P = \frac{D^{\uparrow}(E_F) - D^{\downarrow}(E_F)}{D^{\uparrow}(E_F) + D^{\downarrow}(E_F)} \quad (2)$$

where $D^{\uparrow}(E_F)$ and $D^{\downarrow}(E_F)$ represent respectively the majority and minority states of DOS at the Fermi level (E_F). According to the calculated values, one can deduce that the total polarization of our systems is more interesting in the case of Zr-doped alloys, where the polarization has varied from 93.30% to 68.89% when the concentration x changes from 0.04 to 0.20. While in the case of Ta, the polarization varies from 55.78% to 23.79%. The polarization's values decrease with increasing concentration for both TM. For Zr doped MgTe, the value of the polarization is about 100%, hence its half-metallic character. On the other side, the polarization in the case of Ta is far from 100%, which affirms the metallic behavior of MgTe doped with Ta. When MgTe is doped with Zr, the spindown gap energy decreases with increasing Zr concentration, as shown in Table 2, where the gap values reduce from 1.87 eV at 4% doping to 1.45 eV at 20% doping. This trend indicates a narrowing of the band gap, which can be attributed to the increased hybridization between the Zr d-states and the Te p-states. In contrast, MgTe doped with Ta becomes metallic as mentioned above, with no band gap, highlighting the significant influence of the dopant on the electronic structure and suggesting potential applications in tunable electronic devices.

Table 2. Variation of the wavelength λ_0, the $E_{Formation}$ and Spin-polarization % of $Mg_{1-x}Zr_xTe$ and $Mg_{1-x}Ta_xTe$ compound (x = 0.04, 0. 08, 0.12 and 0.20).

	x %	$\lambda_0(nm)$	$E_g(eV)$	$E_{Formation}$ (eV)	$D^{\uparrow}(E_F)$	$D^{\downarrow}(E_F)$	Polarisation %
Zr	4	663	1.87	-6,0397	0.1955	-0.0067	93.30
Zr	8	729	1.70	-5,8124	0.2990	-0.0108	92.99
Zr	12	810	1.53	-5,5856	0.4109	-0.028	86.99
Zr	20	855	1.45	-5,1458	0.6246	-0.1150	68.89
Ta	4	-	-	-5,9912	0.0637	-0.2246	55.78
Ta	8	-	-	-5,6371	0.2037	-0.3407	25.14
Ta	12	-	-	-5,2842	0.2647	-0.4232	23.04
Ta	20	-	-	-4,6065	0.3621	-0.5884	23.79

The structural stability of the $Mg_{1-x}Ta_xTe$ elements is verified by the formation energies, which is given by the following formula:

$$\boldsymbol{E_{For} = E_T^{Mg1-x(TM)xTe} \; - \; \left[(1-x).E_{Bulk}^{Mg} + x\,.E_{Bulk}^{TM} + E_{Bulk}^{Te}\right]} \quad (3)$$

where x is the doping concentration, $E_T^{\mathrm{Mg1-x(TM)xTe}}$ is the total energy of of $Mg_{1-x}Ta_xTe$ and $Mg_{1-x}Zr_xTe$ compound, $E_{\mathrm{Bulk}}^{\mathrm{Mg}}, E_{Bulk}^{\mathrm{TM}}, E_{Bulk}^{\mathrm{Te}}$is the total energy per atom of Mg, TM, Te respectively. The negative values shown in the table confirm that MgTe doped with concentration x of TM (TM = Zr or Ta) is energetically stable. Increasing concentrations x (x = 0.04, 0. 08, 0.12 and 0.20) of transition metals has a negative impact on compound stability, while in comparison to $Mg_{1-x}Ta_xTe$ elements, $Mg_{1-x}Zr_xTe$ is energetically more favorable.

The variation of photon wavelengths is also cited in Table 2 using the relationship between the gap energy (E_g) and the threshold wavelength of the photoelectric effect ($\boldsymbol{\lambda_0}$) in our alloy Eg (eV). λ_0 (μm) = 1.24. According to the previous study [44], the presence of a wide bandgap (1.75 eV) in pure MgTe gives rise to a wavelength of 709 nm, which belongs to the near infrared (NIR) range according to the International Organization for Standardization (ISO), contrary to the astronomical division where it belongs to the visible range. When we dope with a 4% concentration of Zr, the gap of spin↓ increases, which translates into a decrease in the threshold wavelength of the photoelectric effect to 663 nm, which is in the visible range for the ISO and astronomical divisions. By increasing the percentage to 8%, the wavelength becomes 729 nm and belongs to the NIR in the ISO and the visible domain in the astronomy division. For the concentrations of 12% and 20%, the wavelengths of both divisions are in the NIR range, which allows the appearance of the photoelectric effect in the visible and the near infrared up to 810 nm for 12% and 855 nm for 20%. Other theoretical studies have also examined the internal photoelectric effect in DMS, where doping with 25% Vanadium in CdTe (group IIB-VI) leads to an increase in spin gap ↓ with a decrease in the value of λ_0 [48]. On the other hand, λ_0 decreases respectively with increasing concentrations of TM (Fe, Cr) in the SnC semiconductor of group IV-IV [49], which evolves contrary to our alloy of group IIA-VI, where increasing the concentration led to a higher λ_0 value.

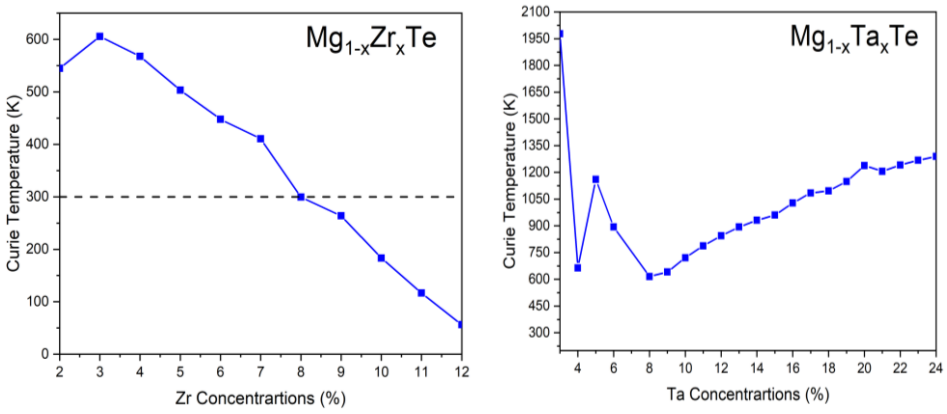

Figure 4. Curie temperature as function of Zr and Ta concentration.

By using the mean field approximation (MFA), the Curie temperature is computed by the following equation [50]:

$$K_B.T_C = \frac{2.\Delta E}{3.x} \quad (4)$$

with K_B is the Boltzmann constant and x is the doping concentration, ΔE is given by the equation (1). In the $Mg_{1-x}Zr_xTe$ case (Figure 4), the maximum Curie temperature (600 K) is observed at a Zr concentration of 3%. Subsequently, it gradually decreases until reaching a Curie temperature (Tc) equal to room temperature at a concentration of 8%, in this concentration range, the component proves worthwhile to be investigated for various spintronic applications. Concentrations below 8% exhibit Tc values lower than room temperature, rendering them unsuitable for spintronic devices. In the $Mg_{1-x}Ta_xTe$ case, the Curie temperature tends to fluctuate at concentrations below 8%. However, it consistently maintains temperatures above room temperature (300 K) for all concentrations. Beyond 8%, the temperature gradually increases, reaching a peak of 1290 K. This characteristic makes $Mg_{1-x}(TM)_xTe$ a compelling candidate for spintronic devices.

CONCLUSION

This study has investigated the electronic and magnetic properties of $Mg_{1-x}(TM)_xTe$ (TM = Zr, Ta) using density functional theory (DFT). Our results indicate that doping with Zr and Ta induces magnetism and alters the electronic structure, with magnetic properties strongly dependent on dopant concentration. The materials are structurally stable, and the ferromagnetic behavior driven by double exchange interaction results in Curie temperatures exceeding 300 K, making these doped systems suitable for room-temperature spintronic applications. Furthermore, the optical properties, particularly in Zr-doped MgTe, show tunable characteristics, essential for optoelectronic uses. The emergence of half-metallic ferromagnetism in Zr-doped MgTe at low concentrations is notable, with Curie temperatures remaining above 300 K. In summary, $Mg_{1-x}(TM)_xTe$ alloys exhibit promising potential for spintronic and optoelectronic applications, offering opportunities for material engineering and advanced device development.

ACKNOWLEDGEMENTS

The authors acknowledge funding from the "Ministère de l'Education Nationale, de la Formation Professionnelle, de l'Enseignement Superieur et de la Recherche Scientifique (Morocco) (MENFPESRS/DESRS)" and the "Ministère de l'Enseignement Supérieur et de la Recherche Scientifique (Tunisie) for the financial support of the research and development project within the framework of Moroccan-Tunisian cooperation (MA-TN 20/PRD-14). The authors also thank the LPHE-MS, Faculty of Sciences, Mohammed V University in Rabat, Morocco for the technical support through computer facilities, where all the calculations have been performed.

REFERENCES

1. Dietl, T. A ten-year perspective on dilute magnetic semiconductors and oxides. *Nat. Mater.* **2010**, 9, 965-974.
2. Dietl, T.; Ohno, H. Dilute ferromagnetic semiconductors: Physics and spintronic structures. *Rev. Mod. Phys.* **2014**, 86, 187.
3. Goumrhar, F.; Cha, F.Z.; Bahmad, L. First principle calculations of electronic and magnetic properties of Cr doped HgSe. *Physica B Condens. Matter* **2019**, 570, 110-115.
4. Sato, K.; Dederics, P.H.; Katayama-Yoshida, H. Curie temperatures of III-V diluted magnetic semiconductors calculated from first principles. *Europhys. Lett.* **2003**, 61, 403.
5. Drissi, L.B.; Benyoussef, A.; Saidi, E.H.; Bousmina, M. Monte Carlo simulation of magnetic phase transitions in Mn-doped ZnO. *J. Magn. Magn. Mater.* **2011**, 323, 3001-3006.
6. Dietl, T.; Ohno, H.; Matsukura, F.; Cibert, J.; Ferrand, D. Zener model description of ferromagnetism in zinc-blende magnetic semiconductors. *Science* **2000**, 287, 1019-1022.
7. Sato, K.; Katayama-Yoshida, H. First principles materials design for semiconductor spintronics. *Semicond. Sci. Technol.* 2002, 17, 367.
8. Zhang, X.; Wu, D.; Geng, H. Heterojunctions based on II-VI compound semiconductor one-dimensional nanostructures and their optoelectronic applications. *Crystals* **2017**, 7, 307.
9. Dietl, T.; Ohno, H.; Matsukura, F. Ferromagnetic semiconductor heterostructures for spintronics. *IEEE Trans. Electron Devices* **2007**, 54, 945-954.
10. Hori, T.; Shiomi, J. Tuning phonon transport spectrum for better thermoelectric materials. *Sci. Technol. Adv. Mater.* **2019**, 20, 10-25.
11. Drissi, L.B.; Bousmina, M.; Fassi-Fehri, O. *Magnetic Skyrmions: Theory and applications*, Online publication, **2021**, DOI: 10.5772/intechopen.96927
12. Chen, J.; Wu, K.; Hu, W.; Yang, J. High-throughput inverse design for 2D ferroelectric Rashba semiconductors. *J. Am. Chem. Soc.* **2022**, 144, 20035-20046.
13. Koo, H. C.; Kim, S.B.; Kim, H.; Park, T.E.; Choi, J.W.; Kim, K.W.; Go, G.; Oh, J.H.; Lee, D. K.; Park, E.S.; Hong, I.S.; Lee, K.J. Rashba effect in functional spintronic devices. *Adv. Mater.* **2020**, 32, 2002117.
14. Malik, G.F.A.; Kharadi, M.A.; Khanday, F.A.; Parveen, N. Spin field effect transistors and their applications: A survey. *Microelectron. J.* **2020**, 106, 104924.
15. Irfan, B. Spintronics: Overview on spin based electronics and its potential applications. *Int. J. Mater. Sci. Appl.* **2021**, 10, 94.
16. Ryu, J.; Lee, S.; Lee, K.J.; Park, B.G. Current-induced spin–orbit torques for spintronic applications. *Adv. Mater.* **2020**, 32, 1907148.
17. Zamani, S.; Farghadan, R. Graphene nanoribbon spin-photodetector. *Phys. Rev. Appl.* **2018**, 10, 034059.
18. Kumar, D.; Chung, H.J.; Chan, J.; Jin, T.; Lim, S.T.; Parkin, S.S.; Sbiaa, R.; Piramanayagam, S.N. Ultralow energy domain wall device for spin-based neuromorphic computing. *ACS Nano*. **2023**, 17, 6261-6274.

19. Elahi, E.; Dastgeer, G.; Nazir, G.; Nisar, S.; Bashir, M.; Qureshi, H.A.; Kim, D.K.; Aziz, J.; Aslam, M.; Hussain, K.; Assiri, M.A.; Imran, M. A review on two-dimensional (2D) magnetic materials and their potential applications in spintronics and spin-caloritronics. *Comput. Mater. Sci.* **2022**, 213, 111670.
20. Bonanni, A. Ferromagnetic nitride-based semiconductors doped with transition metals and rare earths. *Semicond. Sci. Technol.* **2007**, 22, R41.
21. Coey, J.M.D. Magnetism in d^0 oxides. *Nat. Mater.* **2019**, 18, 652-656.
22. El-Achari, T.; Goumrhar, F.; Drissi, L.B.; Laamara, R.A. Structural, electronic and magnetic properties of Mn doped CeO_2: An ab-initio study. *Phys. B: Condens. Matter.* **2021**, 601, 412443.
23. Hori, T.; Shiomi, J. Tuning phonon transport spectrum for better thermoelectric materials. *Sci. Technol. Adv. Mater.* **2019**, 20, 10-25.
24. Yang, J.H.; Chen, S.; Xiang, H.; Gong, X.G.; Wei, S.H. First-principles study of defect properties of zinc blende MgTe. *Phys. Rev. B* 2011, 83, 235208.
25. Zayets, V.; Debnath, M.C.; Ando, K. Complete magneto-optical waveguide mode conversion in Cd1-x Mnx Te waveguide on GaAs substrate. *Appl. Phys. Lett.* **2004**, 84, 565-567.
26. Drief, F.; Tadjer, A.; Mesri, D.; Aourag, H. First principles study of structural, electronic, elastic and optical properties of MgS, MgSe and MgTe. *Catal. Today* **2004**, 89, 343-355.
27. Muthaiah, R.; Garg, J. Thermal conductivity of magnesium telluride (MgTe) – A first principles study. *Solid State Commun.* **2021**, 337, 114414.
28. Duman, S.; Bagcı, S.; Tütüncü, H.M.; Srivastava, G.P. First-principles studies of ground-state and dynamical properties of MgS, MgSe, and MgTe in the rocksalt, zinc blende, wurtzite, and nickel arsenide phases. *Phys. Rev. B*. **2006**, 73, 205201.
29. Debnath, M.C.; Zayets, V.; Ando, K. Thermal annealing of magneto-optical (Cd, Mn) Te waveguides for optical isolators with wider operational wavelength range. *Appl. Phys. Lett.* **2005**, 87, 091112.
30. Kamruzzaman, M.; Luna, T.R.; Podder, J.; Anowar, M.G.M. Synthesis and characterization of Cd1− xCox S thin films prepared using the spray pyrolysis technique. *Semicond. Sci. Technol.* **2012**, 27, 035017.
31. Boulanger, D.; Martin, M.S. Crystal growth and EPR study of Cr+-doped MgTe single crystals. *Phys. Status Solidi*. **1978**, 85, 597-601.
32. Kuhn, A.; Chevy, A.; Naud, M.J. Preparation and some physical properties of magnesium telluride single crystals. *J. Cryst. Growth.* **1971**, 9, 263-265.
33. Behbahani, M.A.; Moradi, M.; Rostami, M. First-principles investigation of electronic, half-metallic, and optical properties of Ti-Doped MgTe semiconductors with various concentrations of dopant. *J. Electron. Mater.* **2018**, 47, 2565-2575.
34. Al-Hawarin, J.I.; Abu-Yamin, A.A.; Abu-Saleh, A.A.A.A.; Saraireh, I.A.; Almatarneh, M. H.; Hasan, M.; Al-Douri, Y. Synthesis, characterization, and DFT calculations of a new sulfamethoxazole Schiff base and its metal complexes. *Materials.* **2023**, 16, 5160.
35. Samia, R.; Yahia, A.; Ahmed, B.; Mokhtar, B.; Noureddine, M.; Mohamed, L.; Al-Douri, Y. Electronic, elastic and piezoelectric properties calculations of perovskite materials type $BiXO_3$ (X = Al, Sc): DFT and DFPT investigations. *Chem. Phys.* **2023**, 573, 111998.
36. Ameri, M.; Bennar, F.; Amel, S.; Ameri, I.; Al-Douri, Y.; Varshney, D. Structural, elastic, thermodynamic and electronic properties of LuX (X = N, Bi and Sb) compounds: First principles calculations. *Phase Transitions.* **2016**, 89, 1236-1252.
37. Zoubir, M.K.; Fadila, B.; Keltoum, B.; Ibrahim, A.; Farah, B.L.; Al-Douri, Y.; Mohammed, A. Structural, electronic and thermodynamic investigation of Ag_2GdSi, Ag_2GdSn and Ag_2GdPb Heusler alloys: First-principles calculations. *Materials Testing.* **2021**, 63, 537-542.

38. Khireddine, A.; Bouhemadou, A.; Alnujaim, S.; Guechi, N.; Bin-Omran, S.; Al-Douri, Y.; Kushwaha, A.K. First-principles predictions of the structural, electronic, optical and elastic properties of the Zintl-phases AE3GaAs3 (AE = Sr, Ba). *Solid State Sci*. *2021*, 114, 106563.
39. Mentefa, A.; Boufadi, F.Z.; Ameri, M.; Gaid, F.; Bellagoun, L.; Odeh, A.A.; Al-Douri, Y. First-principles calculations to investigate structural, electronic, elastic, magnetic, and thermodynamic properties of full-Heusler Rh_2MnZ (Z = Zr, Hf). *J. Supercond. Nov. Magn*. **2021**, 34, 269-283.
40. Akai, H. Fast Korringa-Kohn-Rostoker coherent potential approximation and its application to FCC Ni-Fe systems. *J. Phys. Condens. Matter* **1989**, 1, 8045-8057.
41. Perdew, J.P.; Chevary, J.A.; Vosko, S.H.; Jackson, K.A.; Pederson, M.R.; Singh, D.J.; Fiolhais, C. Atoms, molecules, solids, and surfaces: applications of the generalized gradient approximation for exchange and correlation. *Phys. Rev. B* **1992**, 46, 6671-6687.
42. Akai, H. MACHIKANEYAMA2002v08: Department of Physics, Graduate School of Science, Osaka University, Machikaneyama 1-1, Toyonaka 560-0043, Japan, akai@phys.sci.osaka-u.ac.jp.
43. Noor, N.A.; Ali, S.; Tahiri, W.; Shaukat, A.; Reshak, A.H. First principles study of structural, electronic, and magnetic properties of Mg1-xMnxTe Alloys. *J. Alloys Compd.* **2011**, 509, 8137-8143.
44. Laghrissi, M.; El-Achari, T.; Goumrhar, F.; Mediane, N.; Drissi, L.B.; Ahl Laamara, R. DFT investigations on structural stability and ferromagnetism in V-Doped MgTe for spintronic applications. *Integr. Ferroelectr.* **2023**, 231, 78-88.
45. Akinlami, J.O.; Omeike, M.O.; Akindiilete, A.J. Electronic, structural, and paramagnetic properties of magnesium telluride. *Semicond. Phys. Quantum Electron. Optoelectron.* **2019**, 22, 5-10.
46. Akai, H. Ferromagnetism and its stability in the diluted magnetic semiconductors (In, Mn) As. *Phys. Rev. Lett.* **1998**, 81, 3002-3005.
47. Bondavalli, P. *Graphene and Spintronics, the Good Match in Graphene and Related Nanomaterials.* Elsevier: Online publication; **2018**; pp. 137-156.
48. Essebbahi, L.; Goumrhar, F.; Drissi, L.B.; Es-Semhy, M.; Ahl Laamara, R. first-principles study of the strain effect with half-metallic ferromagnetism in Cd1−xVxTe alloys: Supercell approaches. *Phys. Scr.* **2023**, 98, 035828.
49. Bounouala, Z.; El-Achari, T.; Goumrhar, F.; Drissi, L.B. High Curie temperature in (Fe/Cr)-doped zincblende SnC half-metal ferromagnet: First-principles study. *J. Supercond. Nov. Magn.* **2022**, 35, 1899-1907.
50. Saito, H.; Zaets, W.; Yamagata, S.; Suzuki, Y.; Ando, K. Ferromagnetism in II-VI diluted magnetic semiconductor Zn1−xCrxTe. *J. Appl. Phys.* **2002**, 91, 8085-8087.